Dynamic analysis of a FGM beam with the point interpolation method

***Chaofan Du[1], Xiang Gao[1], †Dingguo Zhang[2], Xiaoting Zhou[1], Junwen Han[1]**

1.College of Civil Science and Engineering, Yangzhou University, Yangzhou 225127, Jiangsu, China
2.School of Science, Nanjing University of Science and Technology, Nanjing 210094, China

*Presenting author:duchaofan@yzu.edu.cn
†Corresponding author: zhangdg419@mail.njust.edu.cn

Abstract

The dynamic characteristics of a hub-functionally graded material beam undergoing large overall motions are studied. The deformation field of the flexible beam is described by using the assumed mode method (AMM), the finite element method (FEM) and the point interpolation method (PIM). Assuming that the physical parameters of functionally graded materials follow certain kind of power law gradient distribution and vary along the thickness direction. The longitudinal deformation and transversal deformation of the beam are both considered, and the nonlinear coupling term which is known as the longitudinal shortening caused by transversal deformation is also taken into account. The rigid-flexible coupling dynamics equations of the system described by three different discrete methods which have a uniform form are derived via employing Lagrange's equations of the second kind. The validity of the point interpolation method established in this paper is verified by comparison with the numerical simulation results of the assumed mode method and the finite element method. On this basis, the influence of functional gradient distribution rules on the dynamic characteristics of flexible beams undergoing large overall motions is discussed. The results show that the assumed mode method cannot deal with large deformation problem. Remaining other physical parameters of functionally graded materials beam unchanged, the maximum displacement of the beam increases with the increase of functionally graded materials index. The natural frequency of transverse bending of beam increases with the increase of rotational speed, when rotational speed is constant, the natural frequency will decrease with the increase of functional gradient index.

Keywords: Point interpolation method; Functionally graded material beam; Rigid-flexible coupled; Natural frequencies

1. Introduction

With the rapid development of science and technology, the disadvantages of traditional materials in heat resistance and strength are more and more obvious, especially in some cutting-edge technologies, such as aerospace engineering, medicine, biological science and so on. In order to meet the needs of practical engineering, it is urgent to meet the needs of new composite materials under complex working conditions. Therefore, functional gradient materials have been proposed by scholars. Functionally gradient materials have the unique advantages in the field of materials, which attracts the attention of scholars all over the world.

In the field of Aeronautics and Astronautics, functional gradient materials are used for helicopter rotors and space manipulators. The behavior of these components can be simplified as large overall motions. Many scholars have applied the assumed mode method, finite

element method, mesh free method, Bezier interpolation method and so on to the deal with discrete problems of flexible body under large overall motions [1]-[8]. The assumed mode method only needs a set of modal functions to describe the deformation of the beam, and does not need to divide several elements along the beam, so it greatly improves the efficiency of programming. However, the limitation of the assumed mode method based on small deformation assumption is illustrated by the example of large deformation [9]. The finite element method needs to divide the deformation field into several elements, and then generate the element shape functions through the element information [10]. The mesh free method overcomes the shortcomings of the above methods. Chaofan Du [11]-[15] applied the mesh free method to the dynamic calculation of beams or plates. The results are compared with the results of the assumed mode method and the finite element method. Therefore, the results of finite element method and mesh free method are more accurate. The natural frequency of the beam with fixed axis rotation motion is studied, and the difference of the natural frequency of different models is obtained [16].

Nowadays, most of the scholars simulate the homogeneous beam with large-scale motion [17]-[20]. The assumed mode method with low accuracy and small application range is used in the dynamic simulation of FGM beams [21]. In this paper, the deformation of FGM beam is described by the point interpolation method (PIM) of mesh free method. Considering the transverse and axial deformation of the beam and the coupling deformation caused by the transverse bending deformation, the rigid flexible coupling dynamic equations of FGM beam are established. The floating coordinate system is used to describe the motion of the system. The second kind of Lagrange equation is used to deduce the dynamic equation of the system, and the simulation program of the rotating FGM beam is compiled. The simulation results of mesh free method (PIM) are compared with those of assumed mode method and finite element method, which shows the correctness and superiority of this method.

2. Dynamic model of rotating FGM beams

2.1 Physical model for rotating FGM beams

Fig.1 shows the central rigid body functional gradient material beam system with fixed axis rotation in the horizontal plane. *OXYZ* is the inertial coordinate system; the radius of the central rigid body is a; the external transmission moment is τ; and the rotational inertia around the axis is J_{oh}. The FGM beam is an equal section beam, and the physical parameters of FGM are: the length of the beam is L, the width is b, and the thickness is h. The floating coordinate system is *Oxy* along the FGM beam. The deformation of any point P on the beam is shown in Figure 1. Different from the traditional homogeneous beam, the physical property of FGM beam distribute along the thickness direction according to a certain power law gradient. In this paper, it is assumed that the elastic modulus $E(y)$ and density $\rho(y)$ of the beam are functions of coordinate y.

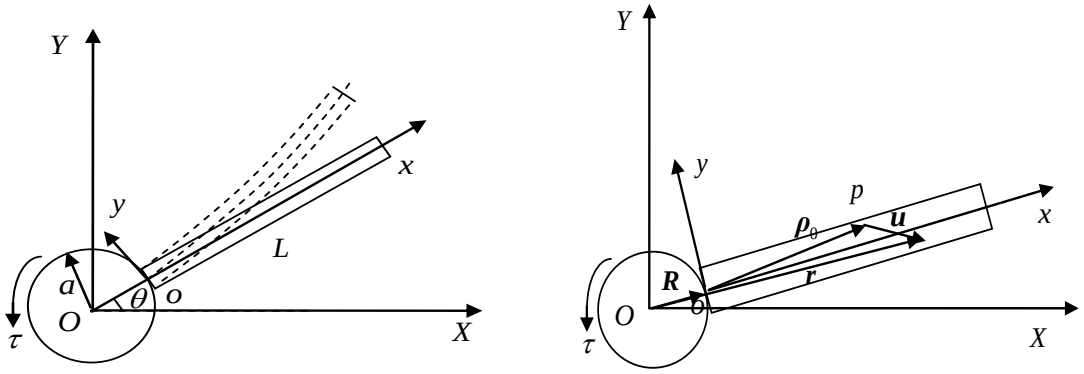

(a) Rigid flexible coupling system (b) Deformation of flexible beam

Fig.1 Deformation diagram of rotating FGM beam

2.2 Kinetic energy and potential energy of the system

In the inertial coordinate system *OXY*, the vector diameter of any point on the FGM beam after deformation is

$$\boldsymbol{r} = \boldsymbol{\Theta}(\boldsymbol{R} + \boldsymbol{\rho}_0 + \boldsymbol{u}) \tag{1}$$

Where

$$\boldsymbol{R} = (a, 0)^{\mathrm{T}} \tag{2}$$

$$\boldsymbol{\rho_0} = (x, y)^{\mathrm{T}} \tag{3}$$

$$\boldsymbol{u} = (u_{x,} u_y)^{\mathrm{T}} \tag{4}$$

$$\boldsymbol{\Theta} = \begin{pmatrix} \cos\theta & -\sin\theta \\ \sin\theta & \cos\theta \end{pmatrix} \tag{5}$$

Where, $\boldsymbol{\Theta}$ is the normal cosine matrix of the floating base relative to the inertial coordinate system, and the deformation vector $\boldsymbol{u}$ in the floating coordinate system can be expressed as:

$$u_x(x, y, t) = w_1 + w_{\mathrm{c}} \tag{6}$$

$$u_y(x, t) = w_2 \tag{7}$$

Where, w_1 is the axial deformation of the flexible beam, w_2 is the deflection of the transverse bending of the flexible beam, and w_c is the shortening of the longitudinal deformation caused by the transverse bending of the flexible beam, i.e. the nonlinear coupling deformation. The expression is:

$$w_{\mathrm{c}}(x, t) = -\frac{1}{2}\int_0^x \left(\frac{\partial w_2}{\partial \xi}\right)^2 \mathrm{d}\xi \tag{8}$$

The velocity of any point of the flexible beam in the inertial coordinate system can be obtained by calculating the first derivative of Eq.(1). It can be expressed as:

$$\dot{\boldsymbol{r}} = \dot{\boldsymbol{\Theta}}(\boldsymbol{R} + \boldsymbol{\rho}_0 + \boldsymbol{u}) + \boldsymbol{\Theta}\dot{\boldsymbol{u}} \tag{9}$$

Therefore, the total kinetic energy of the system can be expressed as:

$$T = \frac{1}{2}\int_V \rho(y)\dot{\boldsymbol{r}}^{\mathrm{T}}\dot{\boldsymbol{r}}\,\mathrm{d}V + \frac{1}{2}J_{\mathrm{oh}}\dot{\theta}^2 \tag{10}$$

According to the continuum mechanics, the longitudinal positive strain ε_{11} at any point *P* of the flexible beam can be derived, and the expression is as follows:

$$\varepsilon_{11} = \frac{\partial w_1}{\partial x} - y\frac{\partial^2 w_2}{\partial x^2} \tag{11}$$

Ignoring the shear and torsion effects of the beam, the deformation potential energy U can be expressed as:

$$U = \frac{1}{2}\int_V E(y)\varepsilon_{11}^2 \mathrm{d}V \tag{12}$$

2.3 Point interpolation method (PIM)

In the discrete field $\boldsymbol{\Omega}$, a continuous function $u(x)$ can be represented by a set of field nodes, and the continuous function $u(x)$ at the calculation point P can be approximately expressed as follows:

$$u(x) = \sum_{i=1}^{m} p_i(x)a_i = \{p_1(x)\ p_2(x)\cdots p_m(x)\}\begin{Bmatrix} a_1 \\ a_2 \\ \vdots \\ a_m \end{Bmatrix} = \boldsymbol{p}^{\mathbf{T}}\boldsymbol{a} \tag{13}$$

In the above formula, $p_i(x)$ is the monomial given by the basis function in the space coordinates $\boldsymbol{x}^{\mathbf{T}}=[x\ y]$, a_i is the undetermined coefficient of $p_i(x)$, and m is the number of monomials. For linear basis function $\boldsymbol{P}^{\mathbf{T}}$ in one dimension (1D) and two dimension (2D) space, it can be expressed as follows:

$$\boldsymbol{p}^{\mathrm{T}}(\boldsymbol{x}) = [1\ x] \quad m = 2\ (1D) \tag{14}$$

$$\boldsymbol{p}^{\mathrm{T}}(\boldsymbol{x}) = [1\ x\ y] \quad m = 3\ (2D) \tag{15}$$

The second basis functions are as follows:

$$\boldsymbol{p}^{\mathrm{T}}(\boldsymbol{x}) = [1\ x\ x^2] \quad m = 3\ (1D) \tag{16}$$

$$\boldsymbol{p}^{\mathrm{T}}(\boldsymbol{x}) = [1\ x\ y\ x^2\ xy\ y^2] \quad m = 6\ (2D) \tag{17}$$

The basis function of order p can be expressed as follows:

$$\boldsymbol{p}^{\mathrm{T}}(\boldsymbol{x}) = [1\ x\ x^2 \cdots x^p] \quad (1D) \tag{18}$$

$$\boldsymbol{p}^{\mathrm{T}}(\boldsymbol{x}) = [1\ x\ y\ x^2\ xy\ y^2 \cdots x^p\ y^p] \quad (2D) \tag{19}$$

In point interpolation, the number of nodes n in the support domain is equal to the number m of the base function, that is, $n = m$. Therefore, the undetermined coefficient a_i in Eq. (13) can be determined by the function $u(x)$ equal to the value on n nodes; that is

$$\left.\begin{aligned} u_1 &= \sum_{i=1}^{m} p_i(x_1)a_i \\ u_2 &= \sum_{i=1}^{m} p_i(x_2)a_i \\ &\vdots \\ u_n &= \sum_{i=1}^{m} p_i(x_n)a_i \end{aligned}\right\} \tag{20}$$

Therefore, Eq. (20) can be expressed as:

$$\boldsymbol{U_c} = \boldsymbol{P_m}\boldsymbol{a} \tag{21}$$

Where

$$\left.\begin{aligned} \boldsymbol{U_c} &= [u_1\ u_2 \cdots u_n]^{\mathbf{T}} \\ \boldsymbol{a} &= [a_1\ a_2 \cdots a_n]^{\mathbf{T}} \end{aligned}\right\} \tag{22}$$

$$\boldsymbol{P_m}=\begin{bmatrix} p_1(x_1)\ p_2(x_1)\cdots\ p_m(x_1) \\ p_1(x_2)\ p_2(x_2)\cdots p_m(x_2) \\ \vdots \quad \vdots \quad \ddots \quad \vdots \\ p_1(x_n)\ p_2(x_n)\cdots p_m(x_n) \end{bmatrix} \tag{23}$$

In the above formula, $\boldsymbol{U_C}$ is the node deformation, and $\boldsymbol{a}$ is the unknown coefficient vector. $\boldsymbol{P_m}$ is dimension and order moment $n\times n$ square matrix.

The unknown coefficient matrix of Eq. (21) can be obtained from *n* equations:

$$\boldsymbol{a}=\boldsymbol{P_m^{-1}U_c} \tag{24}$$

Substituting eq. (24) into eq. (13) can obtain:

$$\boldsymbol{u(x)}=\boldsymbol{P^{\mathrm{T}}(x)P_m^{-1}U_c}=\boldsymbol{\Phi^{\mathrm{T}}(x)U_c} \tag{25}$$

Where, $\boldsymbol{\Psi^{\mathrm{T}}(x)}$ can be expressed as:

$$\boldsymbol{\Phi^{\mathrm{T}}(x)}=\boldsymbol{P^{\mathrm{T}}(x)P_m^{-1}}=\left[\phi_1(x)\ \ \phi_2(x)\ \cdots\ \phi_n(x)\right] \tag{26}$$

PIM shaped functions have *Kronec*ker δ function properties, those properties can be described as:

$$\phi_i(x=x_j)=\begin{cases}1 & i=j \quad i,j=1,2,3\cdots,n \\ 0 & i\neq j \quad i,j=1,2,3\cdots,n\end{cases} \tag{27}$$

Therefore, boundary conditions can be applied in the same way as FEM. In this paper, the corresponding boundary conditions of the cantilever beam are that the longitudinal deformation, transverse deformation and rotation angle of the fixed end of the beam are zero.

In the integration process of PIM, different integration points correspond to different domains, that is, the shape function matrix corresponding to different integration points may be different, which is different from the finite element method. In the finite element method, all integral points in an element are interpolated by the same nodes.

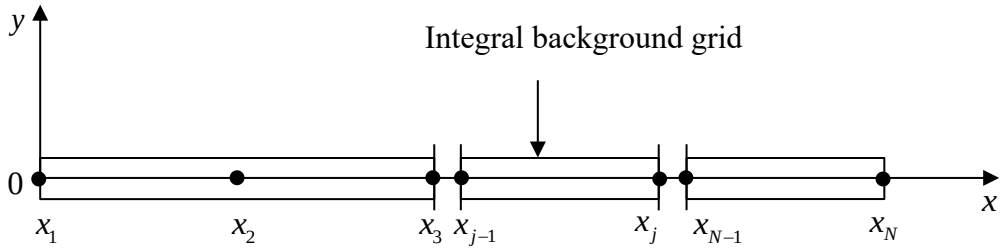

Fig.2 Discretization of FGM beams in mesh free method

The axial and transverse displacement functions of the beam can be expressed as

$$\begin{cases} w_1=\sum_{i=1}^{n}\phi_{xi}u_{xi}=\boldsymbol{\Phi}_x(x)\boldsymbol{A}(t) \\ w_2=\sum_{i=1}^{2n}\phi_{yi}u_{yi}=\boldsymbol{\Phi}_y(x)\boldsymbol{B}(t) \end{cases} \tag{28}$$

Where *n* is the number of nodes in the support region, $\boldsymbol{\Phi}_x(x)$ and $\boldsymbol{\Phi}_y(x)$ are the shape function row matrix of the beam axial and transverse deformation respectively; $\boldsymbol{A}(t)$ is the column vector of the axial deformation of the node with time, and $\boldsymbol{B}(t)$ is the column vector of the lateral deformation and rotation angle of the node with time. They are expressed as

follows:

$$\begin{cases} \boldsymbol{\Phi}_x(x) = (\phi_{x1}\ \ \phi_{x2}\ \ \cdots\ \ \phi_{xn-1}\ \ \phi_{xn}) \\ \boldsymbol{A}(t) = (u_{x1}\ \ u_{x2}\ \ \cdots\ \ u_{xn-1}\ \ u_{xn})^{\mathrm{T}} \\ \boldsymbol{\Phi}_y(x) = (\phi_{y1}\ \ \phi_{y2}\ \ \cdots\ \ \phi_{yn-1}\ \ \phi_{yn}) \\ \boldsymbol{B}(t) = (u_{y1}\ \ u_{y2}\ \ \cdots\ \ u_{yn-1}\ \ u_{yn})^{\mathrm{T}} \end{cases} \tag{29}$$

Where u_{xn} is the axial deformation of the nth node and u_{yn} is the row array composed of the transverse deformation and rotation angle of the nth node. The coupled quadratic term of deformation displacement is as follows:

$$w_c = -\frac{1}{2}\boldsymbol{B}^{\boldsymbol{T}}\boldsymbol{H}(x)\boldsymbol{B} \tag{30}$$

Where $\boldsymbol{H}(x)$ is the coupled shape function, and the expression of the shape function is

$$\boldsymbol{H}(x) = \int_0^x \boldsymbol{\Phi}_y'^{\mathrm{T}}(\xi)\boldsymbol{\Phi}_y^{\mathrm{T}}(\xi)\mathrm{d}\xi \tag{31}$$

Where $\boldsymbol{\Phi}_y'^{\mathrm{T}}(\xi)$ is the first derivative of $\boldsymbol{\Phi}_y^{\mathrm{T}}(\xi)$.

2.4 Dynamic equations

The axial and transverse displacement functions of functionally graded beams are substituted into the expressions of kinetic energy and deformation potential energy of the system, and the generalized coordinates $\boldsymbol{q}$=(θ, $\boldsymbol{A}^{\mathrm{T}}$, $\boldsymbol{B}^{\mathrm{T}}$)$^{\mathrm{T}}$ are taken, using the second kind of Lagrange equation:

$$\frac{\mathrm{d}}{\mathrm{d}t}\left(\frac{\partial T}{\partial \dot{\boldsymbol{q}}}\right) - \frac{\partial T}{\partial \boldsymbol{q}} = -\frac{\partial U}{\partial \boldsymbol{q}} + \boldsymbol{F} \tag{32}$$

$\boldsymbol{F}$=($\boldsymbol{\tau}$,$\boldsymbol{0}$,$\boldsymbol{0}$)$^{\mathrm{T}}$is the generalized force; τ is the principal moment of the resultant external force on the rigid body with respect to the center of mass O of the rigid body. Replace Eqs. (10) and (12) into Eq. (32), After complicated derivation, the dynamic equation can be expressed as:

$$\begin{bmatrix} \boldsymbol{M}_{11} & \boldsymbol{M}_{12} & \boldsymbol{M}_{13} \\ \boldsymbol{M}_{21} & \boldsymbol{M}_{22} & \boldsymbol{M}_{23} \\ \boldsymbol{M}_{31} & \boldsymbol{M}_{32} & \boldsymbol{M}_{33} \end{bmatrix} \begin{bmatrix} \ddot{\theta} \\ \ddot{\boldsymbol{A}} \\ \ddot{\boldsymbol{B}} \end{bmatrix} = \begin{bmatrix} \boldsymbol{Q}_{\theta} \\ \boldsymbol{Q}_{\boldsymbol{A}} \\ \boldsymbol{Q}_{\boldsymbol{B}} \end{bmatrix} \tag{33}$$

The expression of correlation matrix in dynamic equation (33) is as follows:

$$\begin{aligned} \boldsymbol{M}_{11} = J_{\mathrm{oh}} + J_{\mathrm{ob}} + 2\boldsymbol{S}_x\boldsymbol{A} + \boldsymbol{A}^{\mathrm{T}}\boldsymbol{M}_1\boldsymbol{A} + \boldsymbol{B}^{\mathrm{T}}\boldsymbol{M}_2\boldsymbol{B} - \underline{\underline{\boldsymbol{B}^{\mathrm{T}}\boldsymbol{C}\boldsymbol{B}}} - \\ \int_0^L \rho bh[\underline{\underline{\boldsymbol{A}^{\mathrm{T}}\boldsymbol{\Phi}_x^{\mathrm{T}}\boldsymbol{B}^{\mathrm{T}}\boldsymbol{H}(x)\boldsymbol{B}}}]\mathrm{d}x + \frac{1}{4}\int_0^L \rho bh[\underline{\underline{\boldsymbol{B}^{\mathrm{T}}\boldsymbol{H}(x)\boldsymbol{B}\cdot\boldsymbol{B}^{\mathrm{T}}\boldsymbol{H}(x)\boldsymbol{B}}}]\mathrm{d}x \end{aligned} \tag{34}$$

$$\boldsymbol{M}_{22} = \boldsymbol{M}_1 \tag{35}$$

$$\boldsymbol{M}_{33} = \boldsymbol{M}_2 + \int_0^L \rho bh[\underline{\underline{\boldsymbol{H}(x)\boldsymbol{B}\boldsymbol{B}^{\mathrm{T}}\boldsymbol{H}(x)}}]\mathrm{d}x \tag{36}$$

$$\boldsymbol{M}_{21} = \boldsymbol{M}_{12}^{\mathrm{T}} = -\boldsymbol{M}_3\boldsymbol{B} \tag{37}$$

$$\boldsymbol{M}_{31} = \boldsymbol{M}_{13}^{\mathrm{T}} = \boldsymbol{S}_y^{\mathrm{T}} + \boldsymbol{M}_3^{\mathrm{T}}\boldsymbol{A} + \int_0^L \rho bh[\underline{\underline{\boldsymbol{H}(x)\boldsymbol{B}\boldsymbol{\Phi}_y\boldsymbol{B}}}]\mathrm{d}x - \frac{1}{2}\int_0^L \rho bh[\underline{\underline{\boldsymbol{\Phi}_y^{\mathrm{T}}\boldsymbol{B}^{\mathrm{T}}\boldsymbol{H}(x)\boldsymbol{B}}}]\mathrm{d}x \tag{38}$$

$$\boldsymbol{M}_{32} = \boldsymbol{M}_{23}^{\mathrm{T}} = -\int_0^L \rho bh[\underline{\underline{\boldsymbol{H}(x)\boldsymbol{B}\ \boldsymbol{\Phi}_x}}]\mathrm{d}x \tag{39}$$

$$\boldsymbol{Q}_\theta = \tau - 2\dot{\theta}[\boldsymbol{S}_x\dot{\boldsymbol{A}} + \boldsymbol{A}^{\mathrm{T}}\boldsymbol{M}_1\dot{\boldsymbol{A}} + \boldsymbol{B}^{\mathrm{T}}\boldsymbol{M}_2\dot{\boldsymbol{B}} - \underline{\boldsymbol{B}^{\mathrm{T}}\boldsymbol{C}\dot{\boldsymbol{B}}}] + \int_0^L \rho bh[\underline{\underline{\dot{\theta}(2\boldsymbol{A}^{\mathrm{T}}\boldsymbol{\Phi}_x^{\mathrm{T}}\boldsymbol{B}^{\mathrm{T}}\boldsymbol{H}\dot{\boldsymbol{B}} - \boldsymbol{B}^{\mathrm{T}}\boldsymbol{H}(x)\boldsymbol{B}\boldsymbol{B}^{\mathrm{T}}\boldsymbol{H}(x)\dot{\boldsymbol{B}}) - \boldsymbol{B}^{\mathrm{T}}\boldsymbol{\Phi}_y{}^{\mathrm{T}}\dot{\boldsymbol{B}}^{\mathrm{T}}\boldsymbol{H}(x)\dot{\boldsymbol{B}}}}]\mathrm{d}x \quad (40)$$

$$+\dot{\theta}\int_0^L \rho bh\underline{\underline{\dot{\boldsymbol{A}}^{\mathrm{T}}\boldsymbol{\Phi}_x^{\mathrm{T}}\boldsymbol{B}^{\mathrm{T}}\boldsymbol{H}\boldsymbol{B}}}\mathrm{d}x$$

$$\boldsymbol{Q}_A = \dot{\theta}^2\boldsymbol{S}_x^{\mathrm{T}} + 2\dot{\theta}\boldsymbol{M}_3\dot{\boldsymbol{B}} + (\dot{\theta}^2\boldsymbol{M}_1 - \boldsymbol{K}_1)\boldsymbol{A} + \boldsymbol{K}_2\boldsymbol{B} + \int_0^L \rho bh[\underline{\underline{\boldsymbol{\Phi}_x^{\mathrm{T}}\dot{\boldsymbol{B}}^{\mathrm{T}}\boldsymbol{H}(x)\dot{\boldsymbol{B}} - \frac{1}{2}\dot{\theta}^2\boldsymbol{\Phi}_x^{\mathrm{T}}\boldsymbol{B}^{\mathrm{T}}\boldsymbol{H}(x)\boldsymbol{B}}}]\mathrm{d}x \quad (41)$$

$$\boldsymbol{Q}_B = \dot{\theta}^2(\boldsymbol{M}_2 - \underline{\boldsymbol{C}})\boldsymbol{B} - 2\dot{\theta}\boldsymbol{M}_3{}^{\mathrm{T}}\dot{\boldsymbol{A}} - \boldsymbol{K}_3\boldsymbol{B} + \boldsymbol{K}_2^{\mathrm{T}}\boldsymbol{A} - \int_0^L \rho bh[\underline{\underline{2\dot{\theta}(\boldsymbol{H}(x)\boldsymbol{B}\boldsymbol{\Phi}_y\dot{\boldsymbol{B}} - \boldsymbol{\Phi}_y\boldsymbol{B}^{\mathrm{T}}\boldsymbol{H}(x)\dot{\boldsymbol{B}}) + \boldsymbol{H}(x)\boldsymbol{B}\dot{\boldsymbol{B}}^{\mathrm{T}}\boldsymbol{H}(x)\dot{\boldsymbol{B}}}}]\mathrm{d}x \quad (42)$$

$$+\dot{\theta}^2\int_0^L \rho bh[\underline{\frac{1}{2}\boldsymbol{H}(x)\boldsymbol{B}\boldsymbol{B}^{\mathrm{T}}\boldsymbol{H}(x)\boldsymbol{B} - \boldsymbol{H}(x)\boldsymbol{B}\boldsymbol{\Phi}_x\boldsymbol{A}}]\mathrm{d}x$$

The expression of correlation matrix coefficient in kinetic equation (34) ~ (42) is as follows:

$$\boldsymbol{S}_x = \int_0^L \rho bh(R+x)\boldsymbol{\Phi}_x(x)\mathrm{d}x \quad (43)$$

$$\boldsymbol{S}_y = \int_0^L \rho bh(a+x)\boldsymbol{\Phi}_y(x)\mathrm{d}x \quad (44)$$

$$\boldsymbol{M}_1 = \int_0^L \rho bh\boldsymbol{\Phi}_x^{\mathrm{T}}(x)\boldsymbol{\Phi}_x(x)\mathrm{d}x \quad (45)$$

$$\boldsymbol{M}_2 = \int_0^L \rho bh\boldsymbol{\Phi}_y^{\mathrm{T}}(x)\boldsymbol{\Phi}_y(x)\mathrm{d}x \quad (46)$$

$$\boldsymbol{M}_3 = \int_0^L \rho bh\boldsymbol{\Phi}_x^{\mathrm{T}}(x)\boldsymbol{\Phi}_y(x)\mathrm{d}x \quad (47)$$

$$\boldsymbol{C} = \int_0^L \rho bh(R+x)\boldsymbol{H}(x)\mathrm{d}x \quad (48)$$

$$\boldsymbol{K}_1 = \int_0^L E_1 b\boldsymbol{\Phi}_x'^{\mathrm{T}}(x)\boldsymbol{\Phi}_x'(x)\mathrm{d}x \quad (49)$$

$$\boldsymbol{K}_2 = \int_0^L E_2 b\boldsymbol{\Phi}_x'^{\mathrm{T}}(x)\boldsymbol{\Phi}_y''(x)\mathrm{d}x \quad (50)$$

$$\boldsymbol{K}_3 = \int_0^L E_3 b\boldsymbol{\Phi}_y''^{\mathrm{T}}(x)\boldsymbol{\Phi}_y''(x)\mathrm{d}x \quad (51)$$

$$\rho = \int_{-\frac{h}{2}}^{\frac{h}{2}} \rho(y)dy \quad (52)$$

$$E_1 = \int_{-\frac{h}{2}}^{\frac{h}{2}} E(y)dy \quad (53)$$

$$E_2 = \int_{-\frac{h}{2}}^{\frac{h}{2}} E(y)ydy \quad (54)$$

$$E_3 = \int_{-\frac{h}{2}}^{\frac{h}{2}} E(y)y^2dy \quad (55)$$

Where $\boldsymbol{M}_1$、 $\boldsymbol{M}_2$、 $\boldsymbol{M}_3$ are elastic mass matrix; $\boldsymbol{K}_1$、 $\boldsymbol{K}_2$、 $\boldsymbol{K}_3$ are elastic stiffness matrix; and $\boldsymbol{C}$ is the first coupling term.

The FGM studied in this paper consists of ceramic and metal materials, The expression of

gradient distribution is formula (56) and fig. 3.

$$\left.\begin{aligned} E(y) &= (E_{\mathrm{h}} - E_{\mathrm{t}})\left(\frac{2y+h}{2h}\right)^{N} + E_t \\ \rho(y) &= (\rho_{\mathrm{h}} - \rho_{\mathrm{t}})\left(\frac{2y+h}{2h}\right)^{N} + \rho_t \end{aligned}\right\} \tag{56}$$

Where the subscripts h and t represent ceramic and metal materials respectively.

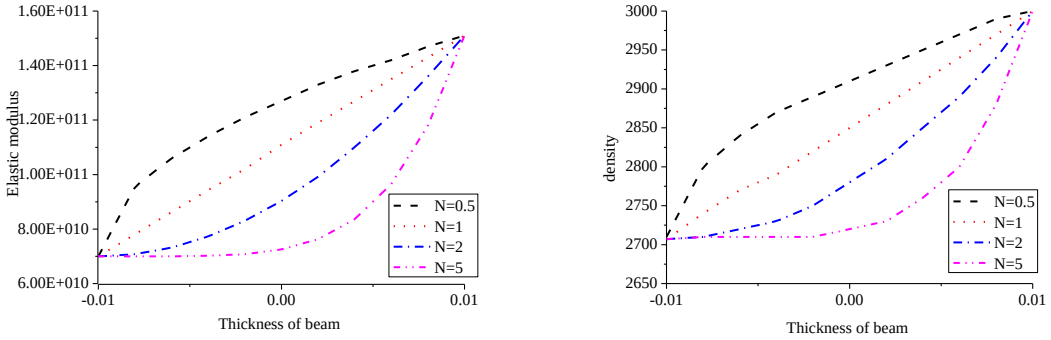

(a) Distribution of elastic modulus (b) Density distribution

Fig.3 Gradient distribution of FGM

By substituting (56) into (52) ~ (55), the expressions of density and elastic modulus are rewritten as:

$$\rho = \frac{\rho_{\mathrm{h}} + N\rho_{\mathrm{t}}}{N+1} \tag{57}$$

$$E_1 = \frac{(E_{\mathrm{h}} - E_{\mathrm{t}})h}{N+1} + E_{\mathrm{t}}h \tag{58}$$

$$E_2 = \frac{(E_{\mathrm{h}} - E_{\mathrm{t}})Nh^2}{2(N+1)(N+2)} \tag{59}$$

$$E_3 = \frac{(N^2+N+2)(E_{\mathrm{h}} - E_{\mathrm{t}})h^3}{4(N+1)(N+2)(N+3)} + \frac{E_{\mathrm{t}}h^3}{12} \tag{60}$$

Equations (34) ~ (42) is the first order model of FGM beam undergoing large overall motions. The first order approximate model of rotating FGM beam is obtained by removing the underlined part.

2.5 Process of coefficient matrix

In the above formulas, J_{oh}, $\boldsymbol{S}_x$, $\boldsymbol{S}_y$, $\boldsymbol{M}_1$, $\boldsymbol{M}_2$, $\boldsymbol{M}_3$, $\boldsymbol{C}$, $\boldsymbol{D}$, $\boldsymbol{K}_1$, $\boldsymbol{K}_2$ and $\boldsymbol{K}_3$ are constant coefficient matrices. Formulas are defined on the global problem domain. In order to calculate the integrals in the above formulas, the whole problem domain should be discretized into a set of integral background grids which do not overlap each other. Taking the distance between two adjacent nodes of the flexible beam as the integral domain, the overall integral can be expressed as

$$\int_{\Omega} \boldsymbol{G}\mathrm{d}\Omega = \sum_{k}^{n_c} \int_{\Omega_k} \boldsymbol{G}\mathrm{d}\Omega \tag{61}$$

Where n_c is the number of integrated background grids, $\boldsymbol{G}$ is the integrand function, and Ω_{k} is the domain of the kth integrated background grid. The Gauss integration method is used to

solve the numerical integration, and n_g Gauss points are used in each integration background grid, and the Eq. (61) is described as

$$\int_{\Omega} \boldsymbol{G} \mathrm{d}\Omega = \sum_{k}^{n_c} \int_{\Omega_k} \boldsymbol{G} \mathrm{d}\Omega = \sum_{k}^{n_c} \sum_{i=1}^{n_g} \widehat{w}_i \boldsymbol{G}(x_{Qi}) \left| J_{ik} \right| \tag{62}$$

Where $\widehat{w}_i$ is the Gauss weighting factor of the ith Gauss integral point x_{Qi}, and J_{ik} is the Jacobi matrix integrating the background grid k at the integration point x_{Qi}.

In order to obtain the numerical solution of each constant matrix, the field nodes in the whole problem domain are numbered from 1 to N. taking the square matrix $\boldsymbol{K}_1$ as an example, The Eq. (49) is described as

$$\boldsymbol{K}_{IJ} = \sum_{k}^{n_c} \sum_{i=1}^{n_g} E_1 b \widehat{w}_i \phi_{xI}^{'\mathrm{T}}(x_{Qi}) \phi_{xJ}^{'}(x_{Qi}) \left| J_{ik} \right| \tag{63}$$

Where

$$\boldsymbol{K}_{IJ}^{ik} = E_1 b \widehat{w}_i \phi_{xI}^{'\mathrm{T}}(x_{Qi}) \phi_{xJ}^{'}(x_{Qi}) \left| J_{ik} \right| \tag{64}$$

Therefore, The Eq. (63) can be described as

$$\boldsymbol{K}_{IJ} = \sum_{k}^{n_c} \sum_{i=1}^{n_g} \boldsymbol{K}_{IJ}^{ik} \qquad I, J = 1, 2, 3, \cdots, N \tag{65}$$

Eqs. (63), (64) and (65) represent the numerical result of the node matrix $\boldsymbol{K}_{IJ}$ obtained by the sum of the contributions of the integral points including nodes I and J in the local support domain. If nodes I and J are not in the local support domain of the integral point x_{Qi}, then $\boldsymbol{K}_{IJ}^{ik}$ is zero. Then the form of $\boldsymbol{K}_1$ is

$$\boldsymbol{K}_1 = \begin{bmatrix} \boldsymbol{K}_{11} & \boldsymbol{K}_{12} & \cdots & \boldsymbol{K}_{1\mathrm{N}} \\ \boldsymbol{K}_{21} & \boldsymbol{K}_{22} & \cdots & \boldsymbol{K}_{2\mathrm{N}} \\ \vdots & \vdots & \ddots & \vdots \\ \boldsymbol{K}_{\mathrm{N}1} & \boldsymbol{K}_{\mathrm{N}2} & & \boldsymbol{K}_{\mathrm{NN}} \end{bmatrix} \tag{66}$$

Similarly, Matrix $\boldsymbol{S}_{\mathrm{y}}$ can be expressed as

$$\boldsymbol{S}_y = \sum_{k}^{n_c} \sum_{i=1}^{n_g} \rho b h \widehat{w}_i (a + x_{Qi}) \phi_{yI}^{\mathrm{T}}(x_{Qi}) \left| J_{ik} \right| \tag{67}$$

Where

$$\boldsymbol{S}_I^{ik} = \rho b h \widehat{w}_i (a + x_{Qi}) \phi_{yI}^{\mathrm{T}}(x_{Qi}) \left| J_{ik} \right| \tag{68}$$

Therefore, The Eq. (67) can be described as

$$\boldsymbol{S}_y = \sum_{k}^{n_c} \sum_{i=1}^{n_g} \boldsymbol{S}_I^{ik} \qquad I = 1, 2, 3, \cdots, N \tag{69}$$

According to the above matrix and array method, the form of matrix in formulas from Eq. (43) to (51) can be obtained.

3. Dynamic simulation

3.1 Model parameters

The specific physical parameters of FGM beam are as follows: E_h=1.51×10^{11}Pa, E_t=7×10^{10}Pa, ρ_h=$3\times10^{3}\mathrm{kg/m^3}$, ρ_t=$2.707\times10^{3}\mathrm{kg/m^3}$. N is the functional gradient index. $l = 5\mathrm{m}$, $b = 2\times10^{-2}\mathrm{m}$, $h = 2\times10^{-2}\mathrm{m}$. In this paper, different discrete methods under the first-order model are simulated.

3.2 Natural frequency of FGM beams

The transverse bending vibration of a flexible beam is usually obvious when the cantilever beam system is rotating undergoing large overall motions, while the longitudinal vibration of the beam can be neglected. Therefore, the transverse bending vibration without considering the influence of longitudinal deformation is studied in this section. In order to simplify the analysis, the large-scale rotation speed is assumed to be uniform, $\ddot{\theta}$=0. By equation (33) the transverse bending vibration equation of the beam can be obtained

$$\boldsymbol{M}_2\ddot{\boldsymbol{B}} + [\dot{\theta}^2(\boldsymbol{C} - \boldsymbol{M}_2) + \boldsymbol{K}_3]\boldsymbol{B} = \boldsymbol{0} \tag{70}$$

Eq. (70) was dimensionless and the following dimensionless variables were introduced

$$\alpha=\mathrm{t/T};\ \beta = x/L\ ;\chi = R/L;\ \delta = B/L \tag{71}$$

$$\gamma = \dot{\theta}T\ ;\phi = E_h/E_t;\ \varphi = \rho_h/\rho_t \tag{72}$$

$$T = (12\rho_t L^4/E_t h^2)^{1/2} \tag{73}$$

Eq. (70) can be rewritten as follows:

$$\bar{\boldsymbol{M}}_2\ddot{\boldsymbol{\delta}} + [\gamma^2(\bar{\boldsymbol{C}}_1 - \bar{\boldsymbol{M}}_2) + \upsilon\bar{\boldsymbol{K}}_3]\boldsymbol{\delta} = \boldsymbol{0} \tag{74}$$

$$\bar{\boldsymbol{M}}_2 = \int_0^1 \left[\boldsymbol{\Psi}_y^{\boldsymbol{T}}\boldsymbol{\Psi}_y\right]d\beta \tag{75}$$

$$\bar{\boldsymbol{C}}_1 = \int_0^1 \left[\beta\bar{\boldsymbol{H}}_1(\beta)\right]d\beta \tag{76}$$

$$\bar{\boldsymbol{H}}_1(\beta) = \int_0^\beta [\boldsymbol{\Psi}_{y,\beta}^{\boldsymbol{T}}\boldsymbol{\Psi}_{y,\beta}]d\upsilon \tag{77}$$

$$\bar{\boldsymbol{K}}_3 = \int_0^1 [\boldsymbol{\Psi}_{y,\beta\beta}^{\boldsymbol{T}}\boldsymbol{\Psi}_{y,\beta\beta}]d\beta \tag{78}$$

$$\upsilon = (\phi - 1)\frac{3(N^2+N+2)}{(N+\varphi)(N+2)(N+3)} + \frac{N+1}{N+\varphi} \tag{79}$$

Table 1 and Table 2 show the variation of transverse bending natural frequency with rotating speed of FGM beam obtained by the assumed mode method, the finite element method and the point interpolation method when the radius of central rigid body is zero. When calculating, the function index is as follow $N = 0.5$; $\phi = 151/70$; $\varphi = 3000/2707$ .It is assumed that the mode method takes the transverse fourth order mode; the finite element method takes 10 elements and the point interpolation method takes 11 nodes. It can be seen from table 1 and table 2 that the first natural frequency increases with the increase of rotation speed. The error between the results of the assumed mode method, the finite element method and the point interpolation method increases with the increase of rotating speed, which indicates that the accuracy of hypothetical modal method will be reduced under high-speed rotation; while the results of the finite element method and the point interpolation method are basically consistent at different speeds, which shows that the point interpolation method can meet the accuracy requirements and the correctness of the method. Fig. 4 shows the comparison of the first and third natural frequencies of transverse bending of the three methods under different non dimensional angular velocity ratios. It can more vividly illustrate that the simulation results of the assumed mode method have more and more errors with the increase of rotating speed. The simulation results of the point interpolation method are basically consistent with those of finite element method.

Table 1. The first order natural frequency with three different discrete methods

Index N	Speed ratio γ	AMM	FEM	PIM
0.5	1	4.4845	4.4846	4.4845
0.5	2	4.5471	4.5471	4.5470
0.5	3	4.6488	4.6487	4.6484
0.5	4	4.7813	4.7803	4.7800
0.5	5	4.9354	4.9326	4.9321
0.5	10	5.9013	5.8553	5.8540
0.5	20	8.0050	7.5431	7.5400

Table 2. The third order natural frequency with three different discrete methods

Index N	Speed ratio γ	AMM	FEM	PIM
0.5	1	78.6623	78.6821	78.6821
0.5	2	78.7407	78.7599	78.7598
0.5	3	79.5085	79.5262	79.5259
0.5	4	80.2414	80.2548	80.2545
0.5	5	80.9592	80.9646	80.9639
0.5	10	88.4284	88.2771	88.2749
0.5	20	113.0945	111.7220	111.7152

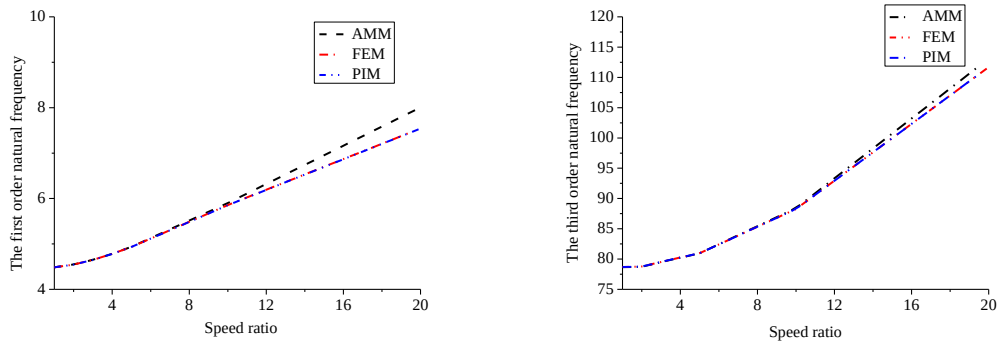

(a) The first order natural frequency (b) The third order natural frequency

Fig.4 Natural frequency

Fig.5 shows the variation of the natural frequency of the FGM beam with the function gradient index obtained by using the assumed mode method, the finite element method and point interpolation method when the radius of the central rigid body is zero and the rotational speed of the FGM beam is constant. The function index is as follow $\gamma = 3$; $\phi = 151/70$; $\varphi = 3000/2707$. It can be found from Fig.5 that when the speed is constant, the natural frequency will decrease with the increase of functional gradient index N, indicating that the greater the flexible beam system, the greater the flexibility, which is consistent with the conclusion shown in Fig. 14.

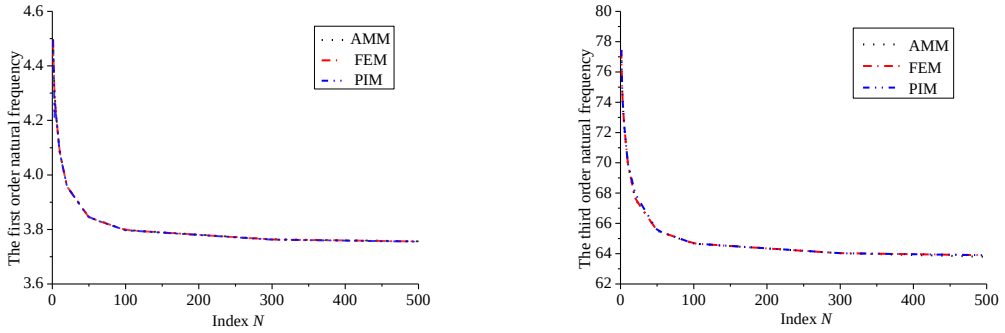

(a) The first order natural frequency (b) The third order natural frequency

Fig.5 Natural frequencies of different functional gradient indices

3.3 Characteristics of system dynamics

The assumed mode method, finite element method and point interpolation method are used to describe the deformation field of the flexible beam. It is assumed that the mode method takes the transverse fourth order mode; the finite element method takes 10 elements and the point interpolation method takes 11 nodes. It is assumed that the law of the large-scale motion of the FGM beam is known

$$\dot{\theta}=\begin{cases}\dfrac{\Omega_1}{T}t-\dfrac{\Omega_1}{2\pi}\sin(\dfrac{2\pi}{t}) & 0\le t\le T\\ \Omega_1 & t>T\end{cases} \tag{80}$$

After 15s, the FGM beam rotates at a constant speed. We first study the difference between the zero-order model (Deleting the underlined items of Eqs. (34)~(42)) and the first-order approximate model (Deleting the double underlined items of Eqs. (34)~(42)). The dynamic characteristics of FGM beams with FGM index N = 2 are studied by taking 4, 10 and 20 rad/s respectively. Then, the dynamic characteristics of the functional gradient index N with 0, 0.5, 1, 2, 5 are studied when the speed is 4rad/s.

Figs. 6~7 show the comparison between the zero-order model (ZOAC) and the first-order model (FOAC) of PIM at different speeds. When the speed is 0.4rad/s, the zero-order model is almost the same as the first-order model. When the speed is 5rad/s, the calculation result of the zero-order model is divergent, and the result of the first-order approximate model is convergent. Therefore, as the speed increases, the calculation results of the first-order approximate model are more reliable.

Figs. 8~13 show the lateral deformation displacement and lateral deformation velocity at the end of flexible beam. The physical parameters are as follows: N = 2, Ω_1=4,10,20 rad/s . It can be seen from the figure that the simulation results of the assumed modal method, the finite element method and the point interpolation method are basically consistent when the speed is low, which indicates the correctness of the model established by the finite element method in this paper. With the increase of the rotating speed, the deviation between the assumed mode method and the finite element method and the point interpolation method becomes larger and larger, and the calculation results of the finite element method and the point interpolation method are almost the same. This is because the hypothetical modal method is based on the hypothesis of small deformation. With the increase of the rotational speed, the deformation is becoming larger and larger, and the error of the hypothetical modal method is bound to increase. It can be seen from the enlarged transverse deformation displacement drawings in each figure that the vibration balance position is not on the beam

axis, but has an offset, and the greater the speed, the more obvious the offset. This is because when N > 0, the metal and ceramic materials are not evenly and symmetrically distributed on both sides of the beam axis, and the axial and transverse coupling potential energy is produced in the calculation of deformation energy.

Fig. 14 shows the variation of lateral deformation of flexible beam end with functional gradient index N. It can be seen that the maximum transverse deformation of the beam end increases with the increase of the functional gradient index N in the process of accelerating the deployment of large-scale motion. It can be seen from the enlarged figure of lateral deformation displacement that when N=0, the material degenerates into homogeneous material, and the vibration equilibrium position is on the beam axis. When N>0, the vibration equilibrium position shifts.

Fig. 15 shows the large lateral bending deformation at the end of the beam. The specific physical parameters are as follows: N=0, E_h=1.51×10^{11}/20Pa , Ω_1=10rad/s . As shown in the figure, the maximum deformation of the beam exceeds 3.2m, which belongs to the case of large deformation. The result of the finite element method and the point interpolation method is converged while the result of the assumed mode method is diffuse.

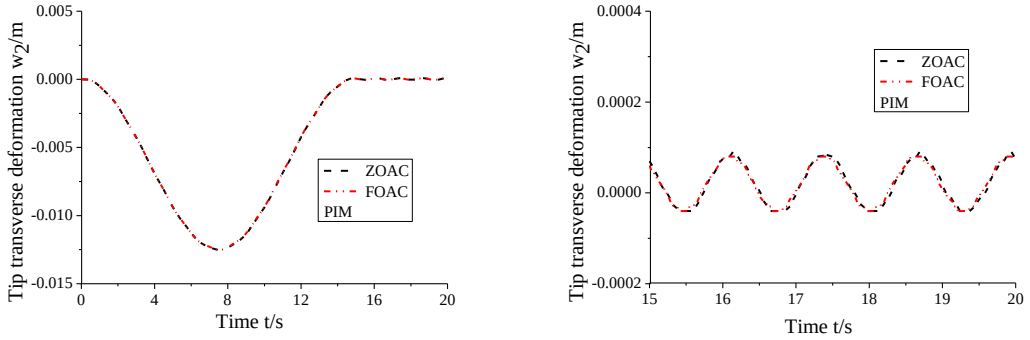

(a) 0～20s Transverse deformation (b) 15～20s Transverse deformation

Fig.6 Comparison of a FOAC model and a ZOAC model (Ω_1 =0.4rad/s)

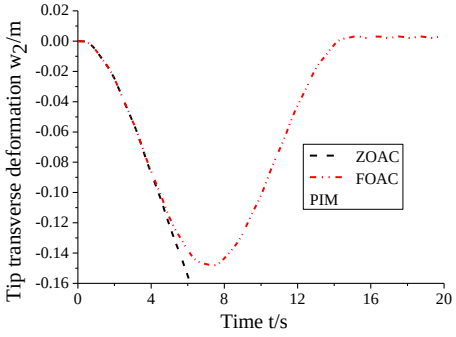

Fig.7 Comparison of a FOAC model and a ZOAC model (Ω_1 =5rad/s)

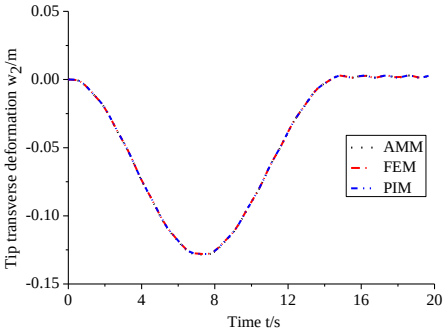

(a) 0～20s Transverse deformation

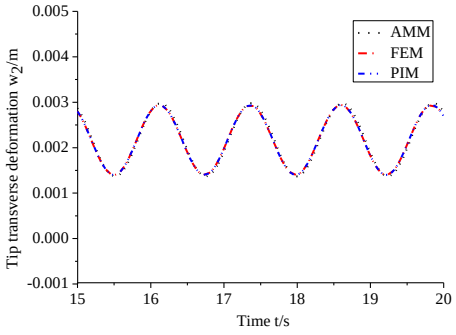

(b) 15～20s Transverse deformation

Fig.8 Tip transverse deformation of the FGM beam(Ω_1 =4rad/s)

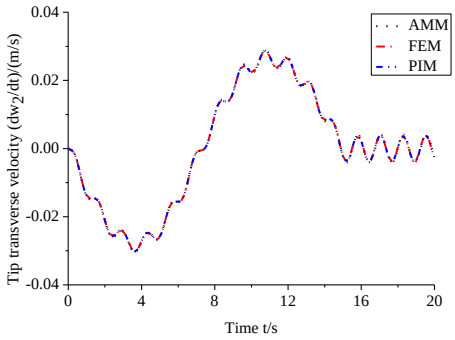

(a) 0～20s Transverse velocity

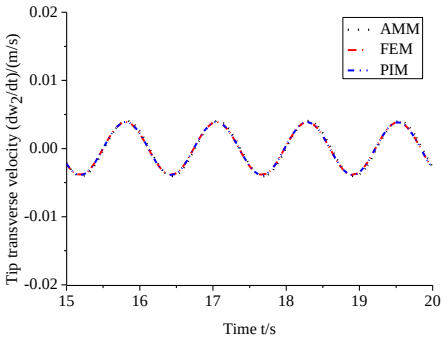

(b) 15～20s Transverse velocity

Fig.9 Tip transverse velocity of the FGM beam(Ω_1 =4rad/s)

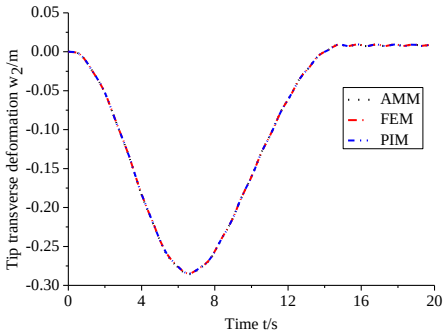

(a) 0～20s Transverse deformation

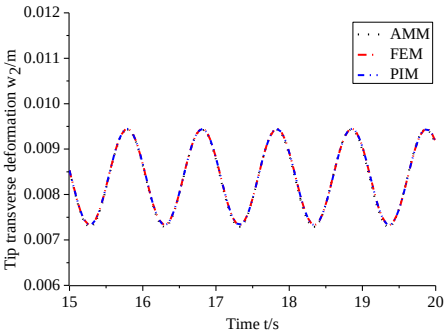

(b) 15～20s Transverse deformation

Fig.10 Tip transverse deformation of the FGM beam(Ω_1 =10rad/s)

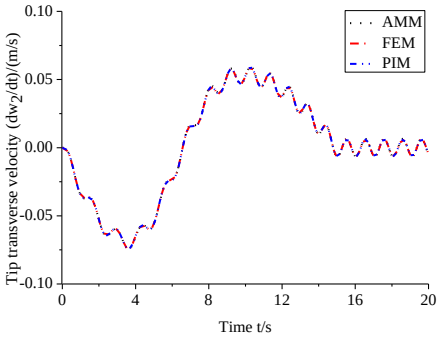

(a) 0～20s Transverse velocity

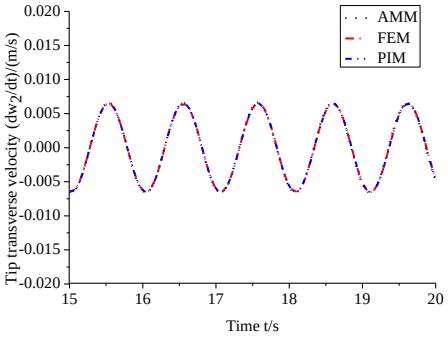

(b) 15～20s Transverse velocity

Fig.11 Tip transverse velocity of the FGM beam(Ω_1 =10rad/s)

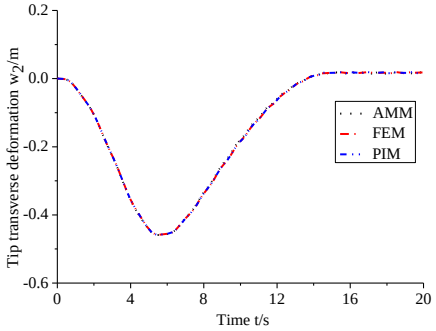

(a) 0～20s Transverse deformation

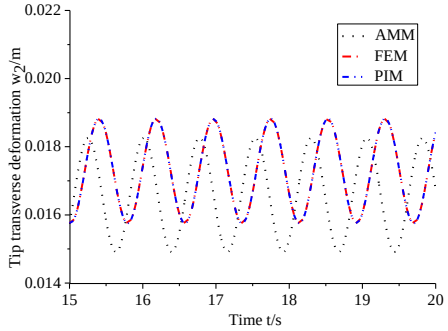

(b) 15～20s Transverse deformation

Fig.12 Tip transverse deformation of the FGM beam(Ω_1 =20rad/s)

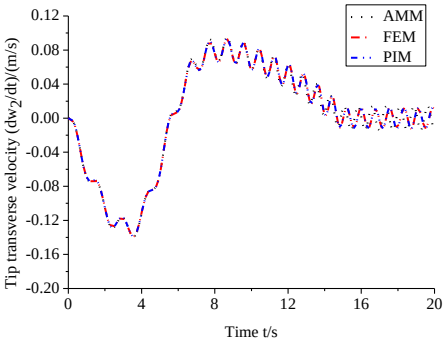

(a) 0～20s Transverse velocity

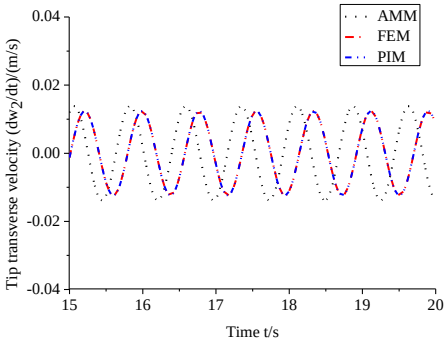

(b) 15～20s Transverse velocity

Fig.13 Tip transverse velocity of the FGM beam(Ω_1 =20rad/s)

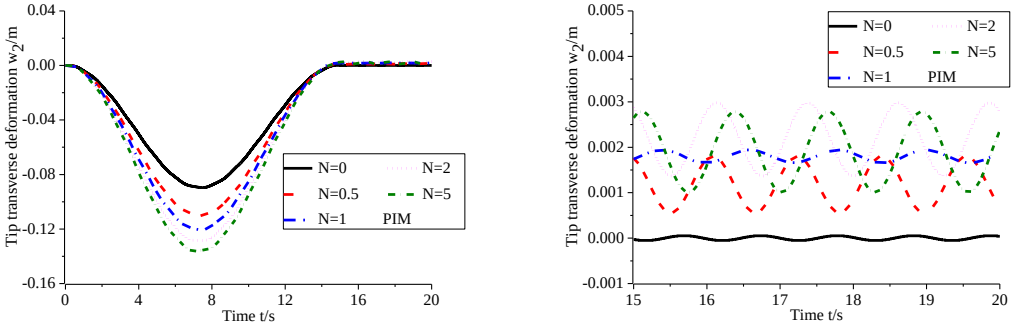

(a) 0～20s Transverse deformation (b) 15～20s Transverse deformation

Fig.14 Tip transverse deformation of the FGM beam(Ω_1 =4rad/s)

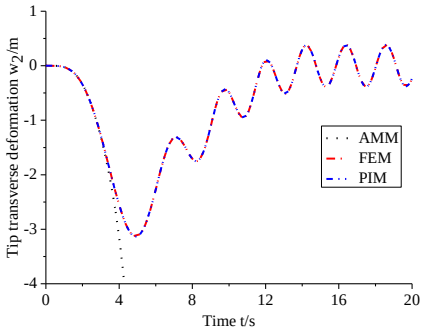

Fig.15 Tip transverse deformation of the FGM beam(Ω_1 =10rad/s)

4. Conclusions

1. The accuracy of the first-order approximate model is better than that of the zero-order model.
2. The maximum tip transverse deformation of the FGM beam increases with the increase of the functional gradient index N. When N>0, the equilibrium position of steady-state vibration will shift and not be on the beam axis.
3. It is assumed that the results of modal method are divergent when the deformation is large, so it can not deal with the problem of large deformation. The results of the finite element method and the point interpolation method are convergent and can be used to solve large deformation problems.
4. The transverse bending natural frequency increases with the increase of rotating speed and decreases with the increase of functional gradient index N.

Acknowledgment

The authors are grateful for the support from the National Natural Science Foundation of China (Grant Nos. 11802263,11272155), the Fundamental Research Funds for the Central Universities of China (Grant No. 30917011103), the Natural Science Foundation of the Jiangsu Province of China (Grant No. BK20180895).

References

[1] Cai G, Hong J. (2005) Assumed mode method of a rotating flexible beam, *Acta Mechanica Sinica* **37**, 48-56.

[2] Jeong S, Yoo H H. (2017) Flexibility Modeling of a Beam Undergoing Large Deflection Using the Assumed Mode Method, *International Journal of Mechanical Sciences* **133**, 611-618.

[3] Yue J, Dong Y, Guedes Soares C. (2018) An experimental-finite element method based on beach marks to determine fatigue crack growth rate in thick plates with varying stress states, *Engineering Fracture Mechanics* **196**, 123-141.

[4] Yoneta S, Koshiba M, Tsuji Y. (1999) Combination of Beam Propagation Method and Finite Element Method for Optical Beam Propagation Analysis, *Journal of Lightwave Technology* **17**, 2398-2404.

[5] Santos C F, Belinha J, Gentil F, et al. (2018) The free vibrations analysis of the cupula in the inner ear using a natural neighbor meshless method, *Engineering analysis with boundary elements* **92**, 50-63.

[6] Sadek S H M, Belinha J, Parente M P L, et al. (2018) The analysis of composite laminated beams using a 2D interpolating meshless technique, *Acta Mechanica Sinica* **34**, 99-116.

[7] Fan J H, Zhang D G. (2014) Bezier interpolation method for the dynamics of rotating flexible cantilever beam, *Acta Physica Sinica Chinese Edition* **63**, 761-761.

[8] Fan J H, Zhang D G. (2012) The Discretization Methods of a Rotating Flexible Cantilever Beam, *Applied Mechanics & Materials* **226-228**, 697-707.

[9] Nobakhti M, Dehkhoda P, Tavakoli A. (2014) Improved modal method of moments technique to compensate the effect of wall dimension in shielding effectiveness evaluation, *Science Measurement & Technology Iet* **8**, 17-22.

[10] Xu G L, Zhang W S, Zhu D B, et al. (2011) Analysis of Residual Stresses Distribution Based on the Finite Element Method for Beam-Column Connections of Steel Frames, *Applied Mechanics & Materials* **71-78**, 4421-4424.

[11] Du C F , Zhang D G, Liu G.R. (2018) A cell-based smoothed finite element method for free vibration analysis of a rotating plate, *International Journal of Computational Methods* **15**, 1840003.

[12] Du C F , Zhang D G, Li L, Liu G.R. (2018) A node-based smoothed point interpolation method for dynamic analysis of rotating flexible beams, *Acta Mechanica Sinica* **34**, 409-420.

[13] Du C F , Zhang D G , Zhang J S , et al. (2019) Predicting Dynamic Behavior of Rotating Mindlin Plate Using Radial Point Interpolation Method, *International Journal of Structural Stability & Dynamics* **19**, 1950070.

[14] Du C.F., Zhang D.G. (2015) Dynamic analysis of rotating cantilever beam based on meshless point interpolation, *Acta Physica Sinica* **64**, 406-415.

[15] Du C.F., Zhang D.G., Hong J.Z. (2015) A meshfree method based on radial point interpolation method for the dynamic analysis of rotating flexible beams, *Chinese Journal of Theoretical and Applied Mechanics*, **47**, 279-288.

[16] He G L, Ding K, Wu X M, et al. (2019) Dynamics modeling and vibration modulation signal analysis of wind turbine planetary gearbox with a floating sun gear, *Renewable Energy* **139**, 718-729.

[17] Wu S.B. *Modeling and simulation of rigid-flex coupling dynamics of flexible beam and flexible thin plate,* Master's Thesis, Nanjing University of Science and Technology, Nanjing, 2009.

[18] Zhang Ch, Fan J.H., Zhang D.G., et al. (2018) Dynamic study of central rigid body-tapered beam system with tip mass, *Chinese Quarterly of Mechanics* **39**, 270-279.

[19] Rezaei V, Shafei A M. (2019) Dynamic Analysis of flexible robotic manipulators constructed of functionally graded materials, *Iranian Journal of Science and Technology, Transactions of Mechanical Engineering* **43**, 327-342.

[20] Sun C Y, Gao H J, He W, et al. (2018) Fuzzy neural network control of a flexible robotic manipulator using assumed mode method, *IEEE Transactions on Neural Networks and Learning Systems* **29**, 5214-5227.

[21] LI L, Zhang D.G., Hong J.Z. (2013) Dynamics of hub-functionally graded material beam system, *Journal of Mechanical Engineering* **49**,77-84.